Low-power inelastic light scattering at small detunings in silicon wire waveguides at telecom wavelengths

Stéphane Clemmen,[1,5,*] Antony Perret,[2] Jassem Safioui,[3] Wim Bogaerts,[4] Roel Baets,[4] Simon-Pierre Gorza,[3] Philippe Emplit,[3] and Serge Massar[1]

[1]*Laboratoire d'Information Quantique, Code Postal 225, Université Libre de Bruxelles (U. L. B.), Boulevard du Triomphe, B-1050 Bruxelles, Belgium*

[2]*Département de Physique, École Normale Supérieure, 24 rue Lhomond, 75005 Paris, France*

[3]*Service OPERA-Photonique, Code Postal 194/5, Université Libre de Bruxelles (U. L. B.), avenue F. D. Roosevelt 50, 1050 Brussels, Belgium*

[4]*Photonics Research Group, INTEC-department, Ghent University—IMEC, Sint-Pietersnieuwstraat 41, 9000 Gent, Belgium*

[5]*Currently with School of Applied and Engineering Physics, Cornell University, Ithaca, New York 14853, USA*

**Corresponding author: sclemmen@ulb.ac.be*

Received March 19, 2012; revised May 29, 2012; accepted June 5, 2012; posted June 6, 2012 (Doc. ID 165029); published July 17, 2012

When a pump beam is propagating through a silicon nanophotonic waveguide, a very small fraction of the light is scattered to other frequencies. At very low intensity, the amount of scattered light is proportional to the power of the pump beam. We show that the scattering intensity increases linearly within the temperature range 300–575 K and that the photon flux decreases as the inverse of the frequency detuning ν over the investigated bandwidth 0.4 THz $< |\nu| <$ 2.5 THz. The simplest interpretation of these observations is that the pump beam is scattered on a one-dimensional thermal bath of excitations. Finally, the implications of this scattering process for quantum optics applications of silicon nanophotonic structures are discussed.

OCIS codes: 290.5820, 130.4310.

1. INTRODUCTION

Light propagation in silicon wire waveguides (SWWs) at telecommunication wavelengths is highly complex. Indeed, such waveguides exhibit an intrinsic Kerr nonlinearity, a Raman scattering with a narrow peak at 15.6 THz, and linear absorption, as well as two photon absorption, which generate free carriers, in turn responsible for free-carrier absorption. Reviews presenting these processes as well as some of their consequences can be found in [1–4].

Recently, SWWs have been investigated as a promising source of correlated photon pairs [5–11]. These are generated via a four-wave mixing process [12] in which the third-order nonlinearity of the medium converts two photons from the pump beam into two correlated photons at frequency detunings $\pm\nu$ from the pump frequency. However, experimental studies of photon pair generation in SWWs have revealed an unexpected photon noise source [5,10]. In particular, the experiment reported in [10] was done in the continuous wave (CW) regime at very low power and was much more sensitive to noise than earlier works. A large reduction from the predicted signal-to-noise ratio (SNR) was then measured (11.3 instead of 69). Some potential sources of noise in SWWs were theoretically studied in [6], but these do not seem to explain the observations of [10]. We note that a similar unexpected source of noise has also been observed in hydrogenated amorphous-silicon waveguides [13].

Here we report on a detailed experimental study of the inelastic light scattering that occurs in SWWs for frequency detunings well below the Raman peak, and we demonstrate that this scattering process is responsible for the low SNR reported in [10]. The spectrum of the scattered light and its dependence on the waveguide temperature is most simply interpreted as scattering on a one-dimensional thermal bath of excitations, involving both absorption and emission of excitations. Finally, time-resolved measurements clearly demonstrate that this scattering is not related to the free-carrier density.

2. EXPERIMENTAL SETUP

Our experiments were performed with SWWs with a lower cladding of silica and air as an upper cladding. The cross section of the waveguide is 500 nm × 220 nm and is monomode at the central wavelength of 1540 nm. These waveguides are 11.2 mm long and are characterized by a group velocity dispersion $\beta_2 = -2 \pm 0.5$ ps^2/m at a wavelength of 1.55 μm and a third-order nonlinear coefficient $\gamma \approx 300$ W^{-1} m^{-1} (assuming an effective area of 0.064 μm^2 and a Kerr coefficient of 4.7×10^{-18} m^2/W [14]). Incoupling/outcoupling is ensured by 10 μm × 10 μm grating couplers etched at the end of an access waveguide whose width narrows down from 10 μm to the nominal width of the waveguide 500 nm along a length of 640 μm. The coupling method allows only coupling with the quasi-TE mode of the waveguide [15] Waveguides are fabricated thanks to inductively coupled plasma-reactive ion etching to etch 220 nm of Si using halogen- and oxygen-based plasma. Etching is done in three steps. First, a thin layer of native oxide is removed, followed by the Si etch, and finally a very selective etch to stop the etch on BOX. During the etch process, polymer is applied to the Si sidewall, but it is removed afterward by using plasma and wet chemical clean (for further details see [16]).

The experimental setup is depicted in Fig. 1 and can be divided into two main parts. The first part (top panel in Fig. 1) is used to generate the scattered flux of photons in the waveguide. The second part (bottom panel in Fig. 1) is an analyzing system to measure the photon flux power, the spectrally resolved photon flux, and the spectrally resolved coincidences. The pump beam is a CW laser beam at 1539.8 nm (Agilent 81600b amplified by a Keopsys ErYb-doped fiber amplifier), which has been cleaned on Stokes and anti-Stokes frequencies using a bandpass filter (BPF). This BPF consists of fiber Bragg gratings, circulators, and 100 GHz commercial add-and-drop filters. It has an extinction larger than 150 dB outside of the pump band (1539.8 ± 0.8 nm). Note that, to reduce as much as possible Raman scattering in the fiber, the pigtail of the last component of the BPF is only 10 cm long. After the BPF, the light is first collimated then injected into the SWW by focusing the beam onto a grating coupler. At the output of the waveguide, the light is coupled into a standard optical fiber by means of a second grating coupler. The input and output coupling losses as well as the linear propagation loss in the waveguide have been measured to be 6 ± 0.5 dB and 2.5 ± 0.5 dB, respectively. After outcoupling, the pump beam is separated by a demultiplexer and sent to a power meter. In the second output port of the demultiplexer, the remaining part of the pump beam is removed by a bandblock filter (bbf) made up of fiber Bragg gratings (extinction greater than 150 dB in the pump band). The Stokes (1542–1558 nm) and anti-Stokes bands (1522–1538 nm) are then separated by a second demultiplexer. Measurements of the photon fluxes in these two bands are carried out with single photon detectors. These detectors are avalanche photodiodes (apds) (ID201 from ID Quantique) operating in Geiger mode at 100 kHz with a gate duration of 100 ns synchronized with a pulse delay generator (Standford DG535). The efficiency of the detectors are $10 \pm 1\%$ (Stokes) and $15 \pm 1\%$ (anti-Stokes) while dark counts are 805 ± 3 Hz and 155 ± 1 Hz, respectively. The temporal resolution of the detectors is limited by the time-to-digital converter (tdc) and is less than 1 ns. For the spectrally resolved measurements, a tunable filter (Gaussian transmission with a full width at half-maximum of 1.5 nm, Newport TBF-1550-1.0) is added in the Stokes arm after the last demultiplexer.

The temperature of the SWW can be varied from 300 K (room temperature) to 575 K thanks to a cartridge heater embedded in the aluminum block holding the waveguide, and its temperature is monitored with a thermocouple. Except when mentioned explicitly, all measurements are carried out at room temperature (≈300 K).

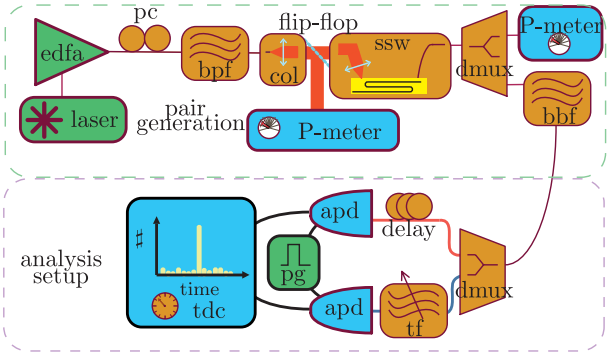

Fig. 1. (Color online) Experimental setup. Photon flux is generated in the top part of the setup and the bottom part is used to analyze this flux in the Stokes and anti-Stokes bands. Laser, CW laser source at 1539.8 nm; EDFA, erbium-doped fiber amplifier; pc, polarization controller; bpf, bandpass filter to clean the pump beam; col, collimation lens; P-meter, power meter; flip flop, mirror used to measure the input power; SWW, silicon wire waveguide; demux, demultiplexer; bbf, bandblock filter; tf, tunable filter; apd, avalanche photodiode; pg, pulse generator; tdc, time-to-digital converter + computer.

3. EXPERIMENTAL RESULTS

The power of the scattered light in the Stokes band was first measured as a function of the input power of the pump laser. As can be seen in Fig. 2, the power in the Stokes band increases with the pump power (P) and exhibits a linear as well as a quadratic dependence with P. The quadratic contribution is well known [10] and can be attributed to the nonlinear third-order Kerr effect. Indeed, when a CW is propagating in a medium, the instantaneous third-order nonlinear effect is responsible for the generation of photon pairs through degenerated four-wave mixing process. The flux of photon pairs emitted over a small frequency interval $\Delta\nu$ at detuning ν from the pump frequency is given by [17]

$$\Phi = \int_{\Delta\nu} \left| \gamma P L \,\mathrm{sinc}\left[\beta_2^{\frac{1}{2}} 2\pi\nu L \left(\frac{\beta_2 (2\pi\nu)^2}{4} + \gamma P \right)^{\frac{1}{2}} \right] \right|^2 \mathrm{d}\nu \qquad (1)$$

and thus increases quadratically with P, while its spectrum $\Phi(\nu)$ has a sinc shape for small frequency interval $\Delta\nu$.

Besides the quadratic contribution to the photon flux, a linear contribution is clearly visible in Fig. 2. This later contribution cannot be explained by nonlinear losses since the power in the waveguide is too small for these losses to be significant. This has been experimentally verified by measuring the propagation losses in the SWW for each data point reported in Fig. 2. The highest relative variation of the ratio of the output to the input power was 2.5% and is attributed to small coupling loss variations.

Raman scattering occurring in the filtering line between the SSW and the detectors is a potential source of photons since this filter is made up of standard optical fiber components. The measurement of this contribution to the total flux was performed by replacing the SWW by a fiber attenuator that introduces the same amount of power attenuation as the

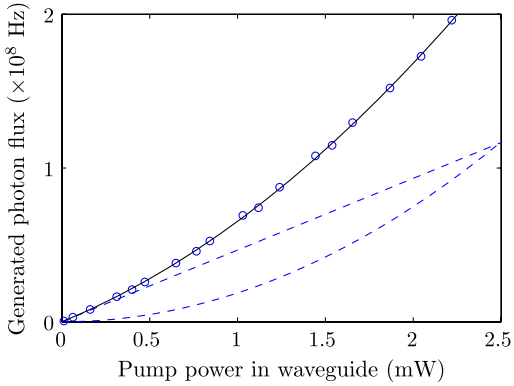

Fig. 2. (Color online) Experimentally recorded photon flux generated in the Stokes band (1541–1558 nm) as a function of the pump power. Solid line, second-order polynomial fit $\Phi = aP^2 + bP$; dotted curves, linear (bP) and quadratic (aP^2) contributions.

SWW. At an input pump power of 1.25 mW (half the maximum power considered in our experiments), the generated photon flux was found to be less than 12% of the total flux in the spectral bandwidth previously considered. Raman scattering in the filtering line cannot therefore account for the difference between the experimentally recorded photon flux and the quadratic law given by Eq. (1).

To identify the physical process responsible for the linear contribution reported in Fig. 2, we experimentally studied the spectral characteristics of the generated photon fluxes in the Stokes and anti-Stokes bands. The spectrally resolved photon flux in these two bands, recorded at a pump power of 250 μW, is shown in Fig. 3(a). As can be seen, the photon fluxes rapidly decrease with the frequency detuning $|\nu|$. These spectra are in agreement with a Bose–Einstein law [solid lines in Fig. 3(a), which are given by Eq. (2)], and support the assumption that photons are scattered by thermal excitations. Moreover, the flux in the Stokes band is larger than its anti-Stokes counterpart. This is expected if the Stokes band is associated with emission of excitations and the anti-Stokes band to absorption of excitations.

To confirm the spectrum presented in Fig. 3(a) is indeed originating from the SWW and is not an artifact of our setup, we performed the same measurement without any sample (i.e., with a fiber attenuator instead of the waveguide). The result presented in Fig. 3(b) shows that there is an inherent noise in our setup whose origin is Raman scattering in the silica fibers between our sample and the filters. Because this later noise is very weak and we wanted to acquire enough data in a reasonable amount of time, we increased the power to 1.25 mW for that measurement. Knowing that the spontaneous Raman scattering grows linearly with respect to the power, we can rescale this flux by a factor 250 μW/1.25 mW = 0.2 [right axis of Fig. 3(b)]. Comparing Fig. 3(a) to the right axis of Fig. 3(b), it appears that, within the studied spectral band, photons generated by Raman scattering in the filtering line account for maximum 25% of the spectral flux up to a detuning of 20 nm. The measurements in Fig. 3(a) were further compared with the spectrum of the correlated photon pairs generated in the SWW. This spectrum was obtained from a coincidence measurement at an increased pump power of 1.75 mW and is shown in Fig. 3(c). It is in agreement with the sinc variation predicted from Eq. (1). For low power ($\gamma PL \ll 1$), the pair spectrum shape is expected to be independent of the power P such that the pair flux scales quadratically with P, thus allowing us to rescale the spectrum by a factor $(250\ \mu\text{W}/1.75\ \text{mW})^2 \simeq 0.02$ [right axis of Fig. 3(c)]. Comparing the scattering flux in Fig. 3(a) to the flux from the right axis in Fig. 3(c), it appears that the flux coming from correlated photons pairs is negligible in comparison with the total flux. In conclusion, the linear contribution of the power dependence of the photon flux generated in the SWW can therefore be attributed to a scattering process whose spectrum is well represented by the measurements reported in Fig. 3(a).

In order to confirm that the scattering process involves interaction with thermal excitations in the SWW, we have measured the evolution of the flux in the anti-Stokes band as a function of the temperature of the waveguide. In this experiment, the input pump power was set to a value of 500 μW, and

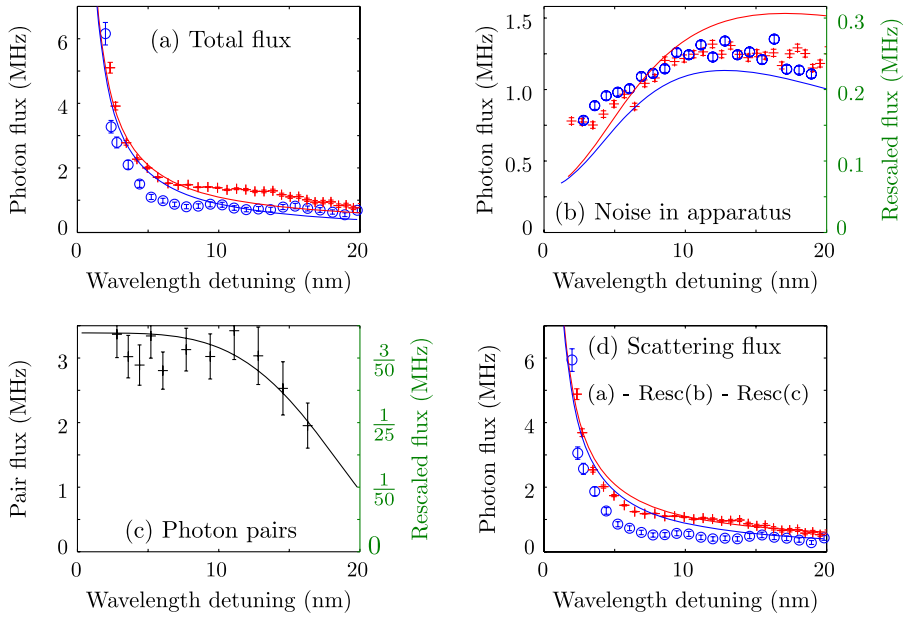

Fig. 3. (Color online) (a) Generated photon flux in the Stokes (plusses) and anti-Stokes (circles) bands (1541.5–1558.5 nm and 1522–1528 nm, respectively), for $P = 250$ μW. The solid curves are theoretical fits with a Bose–Einstein distribution [see Eq. (2)]. (b) Photon flux generated in the filtering line itself at Stokes (plusses) and anti-Stokes (circles) frequencies for input power $P = 1.25$ mW. Solid curves, fit following the Raman noise in a silica fiber. (c) Photon pair flux generated in the silicon waveguide (plusses) and fit following Eq. (1) (curve); input power, 1.75 mW. Error bars are calculated from statistical error as well as error on outcoupling losses. In these figures, the flux for each data point is corrected by subtracting the loss spectrum and dark counts from the detectors. (d) Scattering flux, (a) subtracted by rescaled curves presented in (b) and (c). The fact that the data plotted in (d) are practically identical to those in (a) shows graphically that the scattered photons do not arise from incoupling or outcoupling fibers, nor from photon pair generation. The experiments have been performed at different input powers to ensure similar statistical errors. The left axis refers to the actual power, while the right axis (colored in green) rescales the data to input power $P =$ 250 μW to enable comparison with the spectrum reported in (a) (see discussion in main text).

the total flux generated in the spectral band from 0.4 to 2.5 THz from the pump frequency was recorded. The temperature dependence of the photon flux is shown in Fig. 4 and is found to be linear in the temperature range extending from 300 to 575 K. Note that this flux is corrected for losses and detector efficiency. However, small variations in coupling occur for different temperatures, and this effect was not accounted for in the error bars. We believe these variations explain why the linear fit is not as good as expected.

Free-carrier generation is known to play a major role in the optical properties of SWWs at a wavelength of 1.5 μm and could potentially be involved in the inelastic photon scattering reported in this work. Free carriers arise when electron–hole pairs are created through linear and nonlinear absorption of photons. The free-carrier density is therefore time dependent when pulses are launched in the SWW, and its effects on light scattering can thus be investigated by time-resolved measurements. To study the possible role of free carriers, the CW input beam was cut into square pulses. To achieve this, the output of a pulse pattern generator (Agilent 81110A) was sent through a nonlinear diode that induces sharp rising slopes of the electrical pulses. These electrical pulses drive an integrated lithium-niobate intensity modulator, thereby temporally shaping the input beam into 50 ns square pulses at a 2 MHz repetition rate. The pulse duration and the repetition rate were chosen such that the carrier population can fully build up during each pulse and completely decay between two pulses (the carrier lifetime is ≈1 ns). A fast superconducting single photon detector (Scontel detector, jitter around 40 ps) and high-performance tdc (Agilent Acqirisis system, 5 ps resolution) ensure a time resolution of 80 ps. This overall temporal resolution is limited by the pulse pattern generator but is largely sufficient to reveal any free-carrier effects. The peak pump power has been adjusted so that the linear part of the photon flux is the dominant source of photon generation away from the pump frequency ($P = 0.3, 1.25, 2.5$ mW). This power level also keeps the average number of scattered photons per pulse much lower than 1 to avoid missing late events because of the dead time of the detector. The laser pulses have been measured by the same setup as for the scattered photon flux and are shown in Fig. 5 (bottom curve) together with the photon flux for different input peak powers. As can be seen, the temporally resolved flux of the scattered light is independent of the input power P and exhibits a rise time smaller or equal than 100 ps. This time scale is much faster than the typical values associated with the carrier dynamics in similar waveguides. This latter time ranges between 1 and 4 ns, 1 ns being the commonly accepted value, and 4 ns the carrier lifetime measured in the waveguide used for our experiments at the same power level (note that this value is compatible with [3]). These results clearly show that the inelastic scattering associated with the linear contribution reported in Fig. 2 is not related to the free-carrier density.

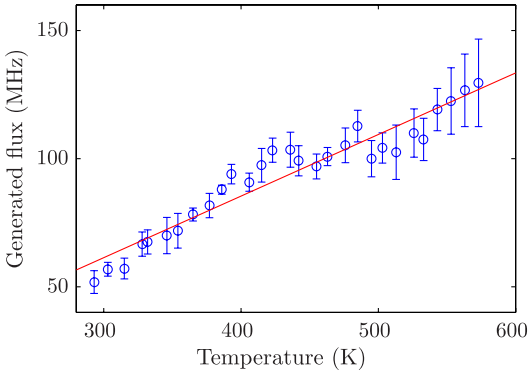

Fig. 4. (Color online) Flux generated in the anti-Stokes band as a function of the SWW temperature (circles) and linear fit (solid line).

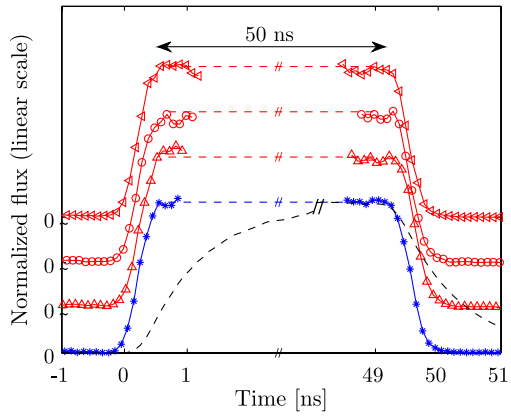

Fig. 5. (Color online) Emitted flux response time. Measured temporal profile of the input pump pulse (asterisks) and corresponding total photon flux emitted at both Stokes and anti-Stokes frequencies [top three (red) curves] for 300 μW (triangles), 1.25 mW (circles), and 2.5 mW (arrows) peak pump power. The black dotted curve shows the temporal dynamic of the carrier density due to the laser pulse assuming a carrier lifetime of 1 ns. Rise/fall time (10%–90%) is the same (450 ps) for both the laser and the three scattered fluxes. The corresponding rise/fall time (10%–90%) of the carrier population is 2.3 ns assuming a 1 ns lifetime. The scattered flux is thus independent of the carrier population.

4. DISCUSSION

We have presented evidence for broadband low-power light scattering in an SWW that exhibits a strong thermal and spectral dependence. In our opinion, the simplest explanation for these observations is an inelastic scattering of the pump beam on a thermal distribution of excitations. This model predicts that the probability for a pump photon at frequency ν_0 to be scattered to frequency $\nu_0 + \nu$ is proportional to the number of excitations with frequency ν. More precisely, assuming a pump beam of power P propagating in a waveguide of length L at a temperature T, the power of the light that is scattered in the frequency interval $\Delta\nu$ around $\nu_0 + \nu$ should have the form

$$P_{\text{scat}} = \kappa\left[\frac{1}{\exp(\mathrm{h}|\nu|/\mathrm{k_b}T) - 1} + \frac{1}{2}(1 - \text{sign}(\nu))\right] L\Delta\nu P, \quad (2)$$

where $\text{sign}(\nu) = \pm 1$ corresponds to Stokes and anti-Stokes scattering, respectively. In general, κ can depend on ν, both through the spectral density of excitations and through the spectral dependency of the scattering amplitude. However, the spectrum reported in Fig. 3(a) is well fitted by Eq. (2) with κ independent of ν (see solid curves in the figure). This suggests that the scattering is on a one-dimensional gas of excitations and that the scattering amplitude varies little with detuning.

We note that, within the investigated range of frequency detunings and temperatures, the Bose–Einstein distribution $(\exp(\mathrm{h}|\nu|/\mathrm{k_b}T) - 1)^{-1}$ is well approximated by $\mathrm{k_b}T/\mathrm{h}|\nu|$, leading to a linear temperature dependence and a spectral variation that scales as the inverse of the frequency detuning. Confirmation of the complete Bose–Einstein distribution predicted by Eq. (2) would require measurements at larger detunings or lower temperature, which is unfortunately not accessible with our setup.

From the data presented in Figs. 2 and 3(c), we estimate that, for the waveguide studied, the proportionality constant is $\kappa = 3.5 \times 10^{-10}$ cm^{-1} THz$^{-1} \pm 30\%$.

The physical origin of the one-dimensional thermal gas of excitations on which the photons scatter is unclear.

Phonons are a natural candidate. However, the phonon dispersion relation in bulk crystalline silicon (see, e.g., [18]) does not allow for the scattering observed here. Another possible explanation is a modification of the continuous dispersion relation of phonons in bulk silicon either through geometrical effects due to the finite dimension of the waveguide or because of the presence of defects in the silicon. Indeed, theoretical study [19] shows that Brillouin scattering can be of importance in nanoscale waveguides due to enhancement via boundary-induced nonlinearities. Explanations based on Raman or Brillouin scattering in the silica substrate beneath the waveguide are probably ruled out because the scattered spectrum would be very different from the observed spectrum [see Fig. 3(c)]. Explanations based on free carriers are also ruled out by our temporal measurements. The fact that a scattering of similar strength was also observed in hydrogenated amorphous-silicon waveguides [13] constrains possible interpretations of our observations.

More insight into the origin of this scattering is expected from a systematic study of the spectrum for various waveguide geometries (especially if the scattering is related to acoustical modes of the waveguide). A spectroscopic characterization of photoluminescence might also be a way to get more information about the origin of the phonon scattering.

The linear broadband scattering studied in the present work is very weak. Nevertheless, it has implications for the future use of SWWs in quantum optics. Indeed our work shows that photon pair sources based on SWWs can be improved, either by cooling the SWW, or (easier) by selecting the Stokes and anti-Stokes spectral bands not too close to the pump wavelength.

We emphasize that, notwithstanding the scattering studied in the present paper noise, SWWs remain a promising source of photon pairs based on four-wave mixing. Indeed, we have estimated that the SNR obtained from coincidence measurements on the SWW and a comparable silica fiber source (silica fibers are the most studied photon pair sources based on four-wave mixing [20–22]) differ by at least a factor of 20. In the case of silica fibers, we made a theoretical estimate based on the theory presented in [23]. For comparison, we tried to keep all other factors constant and in particular assumed zero dispersion for the fiber so that the spectrum of the pair flux is flat, and integrated flux over the same Stokes and anti-Stokes bands as used here. This explains why Raman scattering has plagued photon pair generation experiments based on silica fibers from the onset but has only been noticed recently in the case of SWWs.

ACKNOWLEDGMENTS

We acknowledge the support of the Fonds pour la Formation à la Recherche dans l'Industrie et dans l'Agriculture (FRIA, Belgium) of the Interuniversity Attraction Poles Photonics@be Programme (Belgian Science Policy) under grant IAP6-10 and of the Fonds pour la Recherche Fondamentale Collective (FRFC) of the Fonds de la Recherche Scientifique–Fonds National de Recherche Scientifique (FRS–FNRS) under grant number 2.4608.10. Wim Bogaerts acknowledges the Flemish Research Foundation (FWO-Vlaanderen) for a postdoctoral fellowship.

REFERENCES

1. Q. Lin, O. J. Painter, and G. P. Agrawal, "Nonlinear optical phenomena in silicon waveguides: modeling and applications," Opt. Express **15**, 16604–16644 (2007).
2. R. Claps, D. Dimitropoulos, Y. Han, and B. Jalali, "Observation of Raman emission in silicon waveguides at 1.54 μm," Opt. Express **10**, 1305–1313 (2002).
3. A. C. Turner-Foster, M. A. Foster, J. S. Levy, C. B. Poitras, R. Salem, A. L. Gaeta, and M. Lipson, "Ultrashort free-carrier lifetime in low-loss silicon nanowaveguides," Opt. Express **18**, 3582–3591 (2010).
4. D. R. Solli, P. Koonath, and B. Jalali, "Inverse Raman scattering in silicon: a free-carrier enhanced effect," Phys. Rev. A **79**, 053853 (2009).
5. J. E. Sharping, K. F. Lee, M. A. Foster, A. C. Turner, B. S. Schmidt, M. Lipson, A. L. Gaeta, and P. Kumar, "Generation of correlated photons in nanoscale silicon waveguides," Opt. Express **14**, 12388–12393 (2006).
6. Q. Lin and G. P. Agrawal, "Silicon waveguides for creating quantum-correlated photon pairs," Opt. Lett. **31**, 3140–3142 (2006).
7. H. Takesue, Y. Tokura, H. Fukuda, T. Tsuchizawa, T. Watanabe, K. Yamada, and S.-I. Itabashi, "Entanglement generation using silicon wire waveguide," Appl. Phys. Lett. **91**, 201108 (2007).
8. H. Takesue, H. Fukuda, T. Tsuchizawa, T. Watanabe, K. Yamada, Y. Tokura, and S.-I. Itabashi, "Generation of polarization entangled photon pairs using silicon wire waveguide," Opt. Express **16**, 5721–5727 (2008).
9. K.-i. Harada, H. Takesue, H. Fukuda, T. Tsuchizawa, T. Watanabe, K. Yamada, Y. Tokura, and S.-I. Itabashi, "Generation of high-purity entangled photon pairs using silicon wire waveguide," Opt. Express **16**, 20368–20373 (2008).
10. S. Clemmen, K. Phan Huy, W. Bogaerts, R. G. Baets, Ph. Emplit, and S. Massar, "Continuous wave photon pair generation in silicon-on-insulator waveguides and ring resonators," Opt. Express, 16558–16570 (2009).
11. K.-I. Harada, H. Takesue, H. Fukuda, T. Tsuchizawa, T. Watanabe, K. Yamada, Y. Tokura, and S.-I. Itabashi, "Frequency and polarization characteristics of correlated photon-pair generation using a silicon wire waveguide," IEEE J. Sel. Top. Quantum Electron. **16**, 325–331 (2010).
12. R. W. Boyd, *Nonlinear Optics* (Academic, 1992).
13. S. Clemmen, A. Perret, S. K. Selvaraja, W. Bogaerts, D. van Thourhout, R. Baets, Ph. Emplit, and S. Massar, "Generation of correlated photons in hydrogenated amorphous-silicon waveguides," Opt. Lett. **35**, 3483–3485 (2010).
14. H. K. Tsang and Y. Liu, "Nonlinear optical properties of silicon waveguides," Semicond. Sci. Technol. **23**, 064007 (2008).
15. D. Taillaert, W. Bogaerts, P. Bienstman, T. F. Krauss, I. Moerman, S. Verstuyft, K. De Mesel, and R. G. Baets, "An out-of-plane grating coupler for efficient butt-coupling between compact planar waveguides and single-mode fibers," IEEE J. Quantum Electron. **38**, 949–955 (2002).
16. S. K. Selvaraja, P. Jaenen, W. Bogaerts, D. Van Thourhout, P. Dumon, and R. G. Baets, "Fabrication of photonic wire and crystal circuits in silicon-on-insulator using 193 nm optical lithography," J. Lightwave Technol. **27**, 4076–4083 (2009).

17. E. Brainis, "Four-photon scattering in birefringent fibers," Phys. Rev. A **79**, 023840 (2009).
18. S. Wei and M. Y. Chou, "Phonon dispersions of silicon and germanium from first-principles calculations," Phys. Rev. B **50**, 2221–2226 (1994).
19. P. T. Rakich, C. Reinke, R. Camacho, P. Davids, and Z. Wang, "Giant enhancement of stimulated Brillouin scattering in the subwavelength limit," Phys. Rev. X **2**, 011008 (2012).
20. M. Fiorentino, P. L. Voss, J. E. Sharping, and P. Kumar, "All-fiber photon-pair source for quantum communications," IEEE Photon. Technol. Lett. **14**, 983–985 (2002).
21. H. Takesue and K. Inoue, "Generation of polarization-entangled photon pairs and violation of Bell's inequality using spontaneous four-wave mixing in a fiber loop," Phys. Rev. A **70**, 031802 (2004).
22. X. Li, J. Chen, P. Voss, J. Sharping, and P. Kumar, "All-fiber photon-pair source for quantum communications: improved generation of correlated photons," Opt. Express **12**, 3737–3744 (2004).
23. E. Brainis, S. Clemmen, and Serge Massar, "Spontaneous growth of Raman stokes and anti-Stokes waves in fibers," Opt. Lett. **32**, 2819–2821 (2007).